fluids

MDPI

Article

Thermophysical Properties of Silicon Oxide Nanoparticles in Water and Ethylene Glycol–Water Dispersions

Franz Wittmann *, Zlatan Arnautovic, Florian Heberle and Dieter Brüggemann

Chair of Engineering Thermodynamics and Transport Processes (LTTT), Center of Energy Technology (ZET), University of Bayreuth, Universitätsstraße 30, 95440 Bayreuth, Germany
* Correspondence: franz.wittmann@uni-bayreuth.de

Abstract: Measurements of transmission as well as thermophysical properties have been carried out for different concentrations of SiO_2 nanoparticles (0, 1, 2, 5, 10, and 20 wt.%) in pure water (W) and ethylene glycol–water mixture (EG/W) in a weight ratio of 25/75, from 298 to 323 K at 100 kPa. In particular, the density, specific heat capacity, and thermal diffusivity are measured by a density meter, differential scanning calorimetry, and the laser flash method. In the case of 20 wt.% SiO_2, transmission in the visible range is reduced by 9.3%. Simultaneously, the density rises linearly to 12.3% (in W) and 11.3% (in EG/W). The specific heat capacity decreases to 15.9% (in W) and 17.3% (in EG/W), while the thermal diffusivity rises to 16.4% (in W) and 20.4% (in EG/W). While the density measurements are in very good agreement with the literature, the measured values of the specific heat capacity deviate more than 5%, especially for concentrations below 5 wt.% SiO_2. Moreover, it is shown that the thermal conductivity increases less for fluids in small gaps compared to other authors, which could be due to the suppression of the Brownian motion. Based on the measurement results, temperature- and concentration-dependent correlations for the investigated thermophysical properties are developed using two adjustable parameters. In general, these correlations show deviations of less than 4% from the experimental results, which will help to fill the gaps in the variation of experimental results due to size, SiO_2 nanofluid production, and different measurement devices, and thus optimize solar thermal applications with SiO_2 nanofluid.

Keywords: SiO_2 nanofluid; density; specific heat capacity; thermal diffusivity; thermal conductivity

Citation: Wittmann, F.; Arnautovic, Z.; Heberle, F.; Brüggemann, D. Thermophysical Properties of Silicon Oxide Nanoparticles in Water and Ethylene Glycol–Water Dispersions. *Fluids* **2024**, *9*, 261. https://doi.org/10.3390/fluids9110261

Academic Editor: D. Andrew S. Rees

Received: 9 October 2024
Revised: 30 October 2024
Accepted: 6 November 2024
Published: 8 November 2024

1. Introduction

Global energy consumption has increased dramatically in recent decades. At the same time, efforts are being made to avoid using fossil fuels for energy generation because of global climate change. As a result, the focus is increasingly on renewable energy sources, where solar energy is considered one of the most promising alternatives for satisfying future energy demands, as it is preferable to other renewables in terms of availability, cost, accessibility, capacity, and efficiency [1]. Two different technologies for converting solar energy into usable energy are photovoltaic and solar thermal applications, like concentrating solar power, Fresnel systems, and solar towers. While solar photovoltaic systems convert sunlight directly into electricity, solar thermal systems use a collector to convert solar radiation into thermal energy [2]. Regarding this, the heat transfer fluid is of crucial importance for an efficient application, and, in particular, it is essential for a cost-effective design to know the exact thermophysical properties of the heat transfer fluid.

Nanofluids are an innovative approach to improving thermal efficiency and are recognized as one of the methods for enhancing the performance of solar thermal systems [3–5]. To improve and better predict the heat transfer properties of fluids with nanoparticles, reliable thermodynamic properties as well as improved thermodynamic models and correlations are required.

The origin of the term "nanofluid" is the research of Choi et al. in 1995 and consists of a heterogeneous mixture of solid particles (nanoparticles) in a liquid (base fluid) [6]. Their studies aim to improve the thermal conductivity of water by dispersing various metal oxide nanoparticles in it. The base fluid usually consists of pure fluids such as water (W), ethylene glycol (EG), and propylene glycol, or oils, or various mixtures of these [7]. The particles are solid small particles in the range of 1 to 100 nanometers and they can be chemically stable metals such as Cu or Au, metal oxides such as CuO, SiO_2, TiO_2, ZnO, Al_2O_3, or ZrO_2, or carbons such as graphite, diamond, or graphene [8]. The shape of the particles can vary between spherical, platelets, blades, or bricks [9]. In terms of morphology, a distinction is made between nanoparticles, nanofibers, and nanowires, which are determined by the manufacturing process [10].

Even small concentrations with less than 1 vol.% of nanoparticles in a base fluid can significantly change the thermophysical properties of the fluid. These include improved heat transfer properties such as increased thermal conductivity, which is expected to improve heat transfer in many applications including electronics cooling, engine and proton exchange membrane fuel cell cooling, engine oil transfer, and solar water heating and storage [6,8,11–13].

SiO_2 nanofluids, due to their good rheological behavior and high stability, can achieve good results in increasing heat transfer without significantly increasing pump performance [14]. In addition, SiO_2 nanofluids are expected to transmit sufficient sunlight and offer improved thermophysical properties compared to other nanofluids, which makes them particularly suitable for holistic analysis.

While there are a lot of experimental data on density measurements of various mixtures, fewer data are available for nanofluids. Several authors recognized that the density of nanofluids behaves similarly to a simple linear volumetric mixing rule between the two base materials [15–17]. However, this approach only shows density as a function of concentration and does not take into account the temperature dependence.

The specific heat capacity is also a critical parameter for the applications in question, as it has a direct influence on the heat transfer rate [18]. A higher specific heat capacity allows greater amounts of heat to be stored. At the same time, a higher specific heat capacity ensures greater temperature stability. In the context of long-term heat storage, this translates into a lower energy requirement. In applications characterized by rapid heat-up, such as short-term Fresnel systems, fluids with a lower specific heat capacity are advantageous as they allow the heat transfer medium to respond more quickly. Namburu et al. showed in their investigations that, with 10 wt.% SiO_2, the specific heat capacity is about 12% lower than that of the base fluid for which a mixture of 60/40 wt.% EG/W was used [19]. Vajjha and Das showed that, for 10 vol.% Al_2O_3 and 7 vol.% ZnO, respectively, in a base fluid of 60/40 wt.% EG/W, the decrease in the heat capacity is about 29% and 21%, respectively [20]. For SiO_2 in W, a decrease of 18% in a temperature range of 315 to 363 K is measured for a concentration of 10 vol.% SiO_2 compared to the base fluid. Based on their investigations, Vajjha and Das proposed a new empirical correlation for each of the nanofluids for up to 10 vol.% SiO_2 in W [20].

Kwek et al., Georgia et al., Xie et al., and Bhandari et al. show that the thermal conductivity can be increased with the addition of different nanoparticles in the base fluid [21–24]. Sahoo et al. investigate the thermal conductivity of SiO_2 nanoparticles dispersed in 60/40 wt.% EG/W in a temperature range of 293 to 363 K [25]. The experimental results show that an improvement in thermal conductivity of up to 20% is obtained with a volumetric concentration of 10% at 360 K. In addition, an empirical correlation was also developed based on the obtained data. Ferrouillat et al. considered a wide concentration range up to 34 wt.% SiO_2 in W, and obtained an improvement of 11 to 13% over 293 to 348 K at 34 wt.% [26]. According to Dong et al., the thermal conductivity for SiO_2 in EG/W (50/50) is increased by 6.3% with a concentration of 6 wt.% [27]. Rejvani et al. found that the thermal conductivity with the highest measured concentration of 1.5 wt.% SiO_2 in pure water is enhanced by 4% at a temperature of 333 K [28]. A similar result with

an enhancement of 7.5% for a concentration of 1.5 wt.% SiO_2 in water was published by Mukherjee et al. [29]. The research of Guo et al. showed that the thermal conductivity decreases with an increasing percentage of EG at a constant SiO_2 nanoparticle content in EG/W [30].

In addition to the thermophysical property data, the optical properties of nanofluids are also of great interest for many applications that are using solar energy like direct absorption thermal energy systems. Otanicar et al. developed an experimental setup for determining the extinction index, with respect to the absorption coefficient of water, ethylene and propylene glycol, and Therminol VP-1, commonly used in solar thermal energy applications [31]. Adding nanoparticles, the total extinction coefficient of the nanofluid results from the addition of the extinction coefficient of the base fluid and the extinction coefficient of the particles [32]. In their investigations, Han et al. found that the $Ag/CoSO_4$ nanofluid exhibits strong absorption over a wavelength range from 340 to 600 nm, in contrast to water [33]. In addition to transmission, other properties can also be determined optically. For example, according to Khullar et al., the agglomeration of nanoparticles has no significant influence on the optical properties of amorphous carbon-based nanofluids [34]. To apply this knowledge to solar thermal systems, the accurate characterization of all these thermophysical properties is required for system design. However, the available data are still limited, which is reflected in the small number of experimental measurement data of individually measured thermophysical properties. Due to the different production, various nanoparticle sizes, and different concentrations, as well as base fluids, the holistic consideration of several properties of the same SiO_2 nanofluid in a wide concentration range is of particular interest.

To extend the database of SiO_2 nanofluids, the present work focuses on providing experimental data for the density, specific heat capacity, and thermal conductivity, as well as the optical properties, transmission, and absorption, of SiO_2 nanoparticles in W and EG/W (25/75). The thermophysical properties are measured in a temperature range of 293 to 323 K at 1 bar with a density meter, differential scanning calorimetry, and a laser flash analysis. The optical properties are measured with two spectrometers at 293 K. The measurement results obtained provide an improved analysis of SiO_2 concerning its solar thermal applications and are used to develop a new empirical correlation.

2. Experimental Section

In the following, the experimental setups and evaluation methods concerning the properties of the density, specific heat capacity, thermal conductivity, and optical property transmission, as well as the absorption coefficient, are presented and discussed.

2.1. Investigated Fluids and Sample Preparation

The base fluids are distilled water and ethylene glycol, which are also used for validation purposes. Nanografi Nano Technology supplied the investigated nanofluids. Detailed information is provided in Table 1. The dispersions of nanofluid with a concentration of 22 wt.% are diluted to 1, 2, 5, 10, and 20 wt.% concentrations by adding water or ethylene glycol. The mass fractions are accurately determined using a precision balance (SARTORIUS CUBIS semi-microbalance 225P, Sartorius Lab Instruments, Göttingen, Germany) with a measurement uncertainty of 0.01 mg. A syringe is used to add the components one at a time, and a 0.4 mm-diameter syringe needle is used for fine dosing. The nanofluids are then sonicated for 30 min using the ultrasonic device UP200Ht from Hielscher (Teltow, Germany). The manufacturer's specifications regarding the nanoparticle size are verified using a ZEISS LEA 1530 scanning electron microscope with a Schottky field emission cathode from the Bavarian Polymer Institute (BPI) (ZEISS, Jena, Germany). A high-resolution image of the pure nanoparticles is shown in Figure 1. The results of the images show that an average nanoparticle size of 28 nm can be confirmed.

Table 1. Information and properties of the investigated components.

Chemical Name	CAS Number	Purity (%)	Particle Size (nm)	Density at 25 °C (g/cm^3)	Specific Heat Capacity at 25 °C (kJ/kgK)	Thermal Conductivity at 25 °C (W/mK)
Water (H_2O)	7732-18-5	>99.95	-	0.997 [a]	4.181 [a]	0.607 [a]
Ethylene glycol ($C_2H_6O_2$)	107-21-1	99.5	-	1.110 [a]	2.412 [a]	0.252 [a]
Silicon dioxide (SiO_2)	7631-86-9	99.5	28	2.650 [b]	0.680 [b]	1.400 [b]

[a] REFPROP v.10.0 [35]; [b] Mukherjee et al. [29].

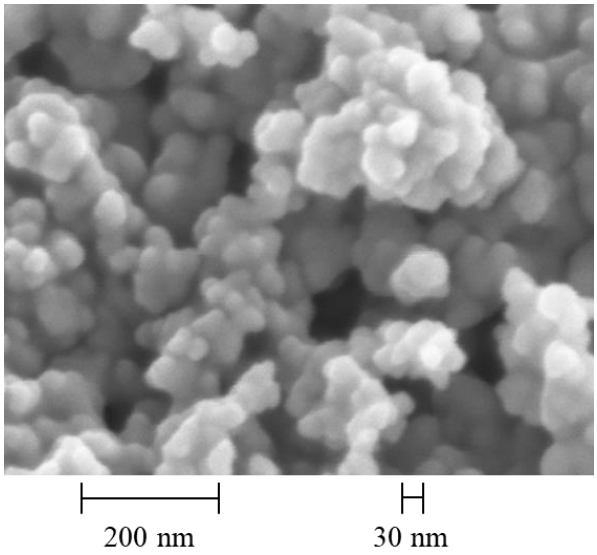

Figure 1. Images of the SiO_2 nanoparticles in powder form with a resolution of 200 nm.

It also shows that the particles in powder form tend to agglomerate easily, which then dissolve again in the base fluid. In addition, spectra, as shown in Figure 2, are recorded for all concentrations using the INVENIO R Fourier-transform infrared spectrometer from Bruker (FT-IR) (Ettlingen, Germany). In the wavenumber k′ range of 800 to 1200 cm^{-1}, different absorption lines are visible for water, ethylene glycol, and SiO_2 nanoparticles.

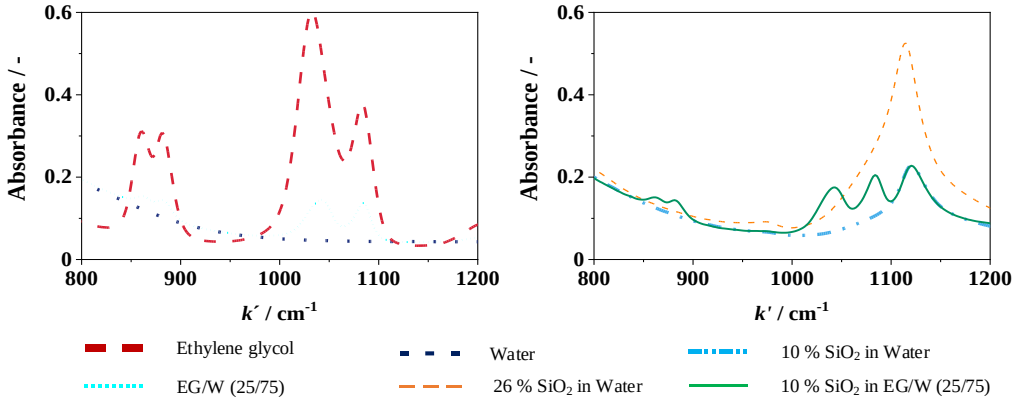

Figure 2. Spectra of different concentrations of SiO_2 in W (**left**) and EG/W (25/75) (**right**) using FT-IR.

To exclude mixing errors and to verify whether the mixture remains stable, additional spectra were recorded in 1% steps and the samples were measured before and after the measurements. The maximum relative deviation of the FT-IR is 0.4 wt.%. The measurement results before and after the tests were within this deviation.

2.2. Apparatus and Procedure

The examined thermophysical properties and transmission of SiO_2 in water, EG, and water/EG mixtures are determined in the temperature range of 293 to 323 K and 100 kPa using the measurement devices described below.

2.2.1. Transmission

The experimental setup for transmission measurements can be seen in Figure 3. Two spectrometers with a total wavelength range of 300 to 1700 nm are used to cover the majority of solar radiation. The light source with a wavelength range of 350 to 2700 nm is connected to the cuvette holder, in which the liquid sample is contained, via a fiber optic cable. After transmission through the cuvette, the remaining radiation is detected by the Ocean Insight FX-XR1-ES spectrometer with a wavelength range of 300 to 1000 nm and the Ocean Insight NIRQuest+1.7 with a wavelength range of 900 to 1700 nm via a y-fiber optic cable (Ocean Insight, Orlando, FL, USA).

Figure 3. Experimental setup for transmission determination with two spectrometers, OCEAN-FX and NIRQuest.

The cuvette is a high-precision cell quartz glass cuvette from Hellma Analytics with a light path of 10 mm. Three measurements are taken of each sample. The evaluation is carried out according to the following physical context. When the radiation hits the fluid, a certain proportion of the radiation dI is removed from the beam direction at an infinitesimal distance of $z + dz$ so that the following equation applies [36]:

$$dI = -\alpha_{\mathrm{Ext}} \times I \, dz \tag{1}$$

where α_{Ext} is the absorption coefficient. If scattering is very small, multiple scattering can be ignored and Equation (1) can be integrated into

$$I_{\mathrm{T}} = I_0 \times e^{-\alpha_{\mathrm{Ext}} \times l_{\mathrm{Abs}}} \tag{2}$$

with I_{T} for the transmitted radiation, I_0 for the original radiation, and l_{Abs} for the path the radiation has passed through.

2.2.2. Density

The density of the nanofluids is measured by a density meter 4200 M (DMA) test setup from Anton Paar, as shown in Figure 4. With the pulsed excitation method, the mechanical oscillation of an oscillating U-tube filled with the test medium is converted into an alternating voltage of the same frequency.

The oscillation period τ is related to the density ρ of the sample in the transducer as follows:

$$\rho = A \times \tau^2 - B \tag{3}$$

with A and B being transducer constants, which are determined by calibrating two known substances with their densities ρ_1 and ρ_2 by

$$A = \frac{\rho_1 - \rho_2}{\tau_1^2 - \tau_2^2} \tag{4}$$

$$B = \frac{\tau_2^2 \times \rho_1 - \tau_2^2 \times \rho_2}{\tau_1^2 - \tau_2^2} \quad (5)$$

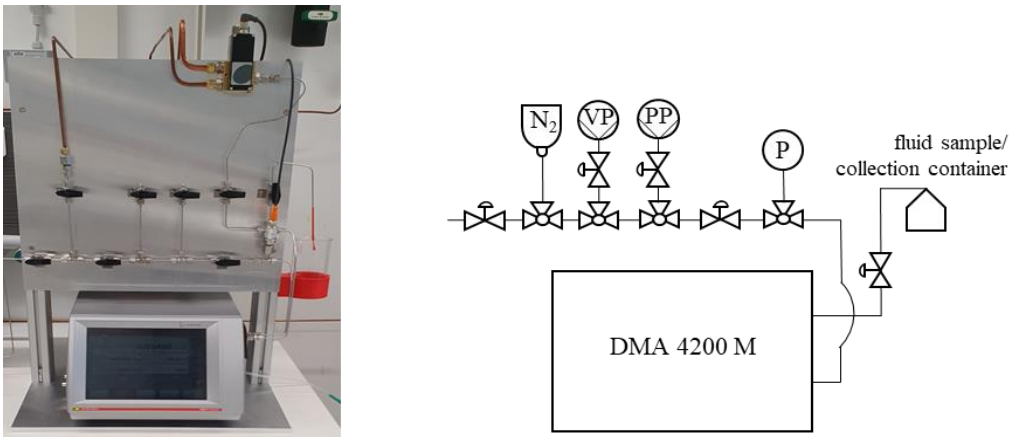

Figure 4. Experimental setup for density determination with a DMA 4200 M.

The DMA is capable of measuring density from 0 to 3 g/cm^3 at temperatures from 263 to 423 K with an accuracy of ±0.03 K [37] and at pressures of up to 500 bar. The pulsed excitation method provides very stable density and a viscosity correction eliminates the influence of viscosity, giving density results accurate to 0.0002 g/cm^3.

Before measurements, the entire system is flushed with ethanol and nitrogen (N_2). To avoid possible bubble formation due to the heating of the liquid sample in the measurement cell, the liquid sample is preheated and then filled into the heated measuring cell. Optionally, a vacuum pump (VP) and a pressure pump (PP) can also be connected to carry out measurements at different pressures.

Measurements are always taken at the highest temperature and then the cell is cooled in 5 K steps. A preset time of 20 min ensures that the measured value is stationary. The pressure in the system is monitored by a pressure sensor. The density measurements were repeated three times.

2.2.3. Differential Scanning Calorimetry

The heat flux differential scanning calorimetry 200 F3 Maia (DSC) from Netzsch (Selb, Germany) is used to determine the heat capacities of the fluids, as seen in Figure 5.

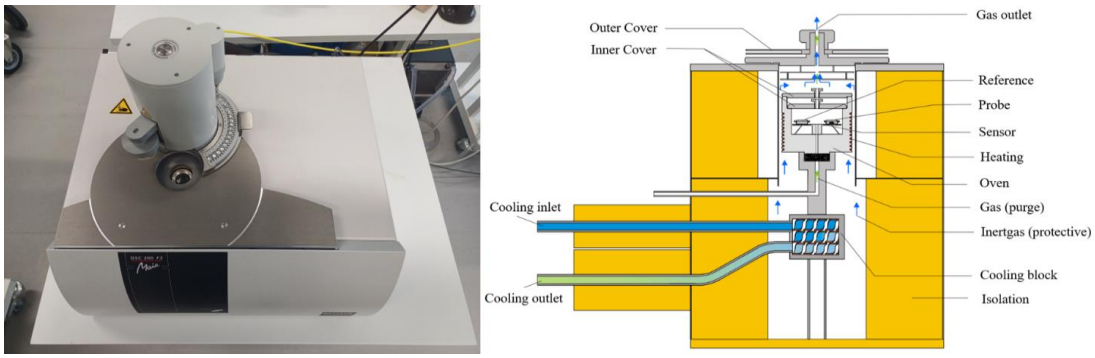

Figure 5. Experimental setup for specific heat capacity determination with a DSC 200 F3 Maia [38].

Samples are filled in an aluminum crucible. The temperature of the sample is adapted by an oven. The measurement principle is divided into three steps. First, the heat flow rate of the baseline θ_0 is determined by measuring an empty aluminum crucible, as a reference.

Second, as a calibration, a sapphire as a reference mass with a known heat capacity is measured in the same crucible, resulting in the following equation:

$$C_{\mathrm{Ref}} \times m_{\mathrm{Ref}} \times \beta = K_{\theta}(T) \times (\theta_{\mathrm{Ref}} - \theta_0) \tag{6}$$

with the reference heat capacity C_{Ref} of the known substance, the reference mass m_{Ref}, and the heat rate β. The temperature-dependent function $K_{\theta}(T)$ serves as the calibration. In the third step, approximately 30 mg of the sample is sealed in the aluminum crucible and measured, which leads to

$$C_S \times m_S \times \beta = K_{\theta}(T) \times (\theta_S - \theta_0) \tag{7}$$

where the index "S" stands for the sample [39]. The comparison of Equations (6) and (7) results in

$$C_S = \frac{(\theta_S - \theta_0)}{(\theta_{\mathrm{Ref}} - \theta_0)} \times \frac{m_{\mathrm{Ref}}}{m_S} \times C_{\mathrm{Ref}}, \tag{8}$$

The measurements are performed under a nitrogen atmosphere at 100 mL/min and are repeated 5 times per sample. The measured temperature range is between 287 and 333 K. The accuracy of the measured heat capacity can be considered in a range of ±3% [38]. The calibration of temperature is carried out with pure water, gallium, indium, bismuth, and zinc with a deviation of 0.1 K.

2.2.4. Laser Flash Analysis

To determine the thermal conductivity, a Netzsch Laser Flash Analysis device (LFA 447) is used. The sample is irradiated uniformly on one side with a light pulse from a xenon flash lamp. The temperature increases on the opposite side and is measured as a function of time using an IR detector cooled with liquid nitrogen. Using the sample thickness l and the half-time of the temperature rise t_{50}, the thermal diffusivity a is calculated from the following equation [40]:

$$a = 0.1388 \times \frac{l^2}{t_{50}}. \tag{9}$$

A triple-layer sample holder, which is shown in Figure 6, is used for low-viscosity samples such as water. The fluid sample, which is 200 µL, forms the middle layer.

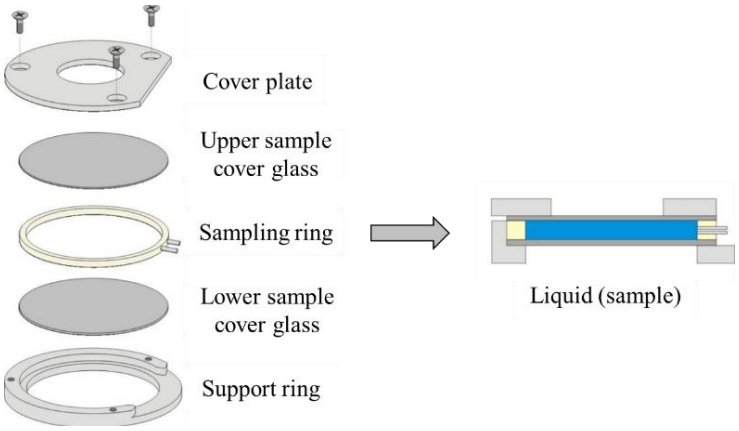

Figure 6. Sample holder of the LFA [40].

The device of the Netzsch Laser Flash Analysis device (LFA 447) is shown in Figure 7. The fluid is surrounded on both sides by an aluminum sample cover plate, which is coated on the outside with a layer of graphite. The thermal diffusivity is measured 5 times per sample from 298 to 323 K with a 5 K interval.

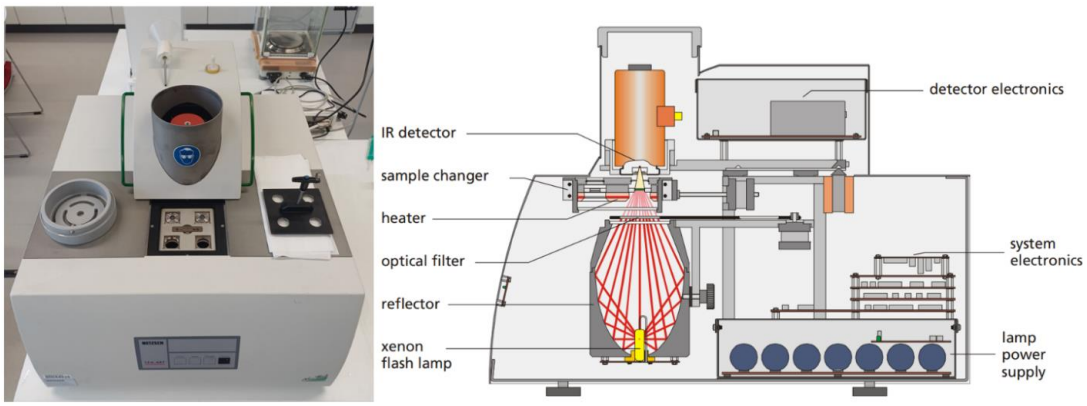

Figure 7. Experimental setup for thermal diffusivity determination with a LFA 447 [40].

Considering the density ρ and the specific heat capacity c_p, the thermal conductivity λ can be calculated according to

$$\lambda = a \times \rho \times c_p. \tag{10}$$

3. Correlations

In this chapter, correlations for the estimation of the considered thermophysical properties of the nanofluids are presented and discussed. Existing approaches calculate the properties as a function of concentration and temperature.

3.1. Density

In general, the density is expressed as the ratio of mass m to volume V. Pak and Cho developed an approach to determine the density of a nanofluid:

$$\rho_{nf} = \left(\frac{m}{V}\right)_{nf} = \frac{m_{bf} + m_{np}}{V_{bf} + V_{np}} = \frac{\rho_{bf} V_{bf} + \rho_{np} V_{np}}{V_{bf} + V_{np}} = \left(1 - \phi_{np}\right) \times \rho_{bf} + \phi_{np} \times \rho_{np} \tag{11}$$

as a function of the nanoparticle concentration ϕ_{np} where the indices "bf" and "np" stand for the base fluid and nanoparticle, respectively [15]. It consists exclusively of non-empirical parameters and is widely applied for any concentration of nanoparticles in any base fluid.

3.2. Specific Heat Capacity

For the calculation of the specific heat capacity of nanofluids, there are only a few correlations in the literature available. Pak and Cho established a correlation based on the volume fraction of the nanoparticle in the base fluid using the mixing rule:

$$C_{p_{nf}} = \phi_{np} \times C_{p_{np}} + \left(1 - \phi_{np}\right) \times C_{p_{bf}}, \tag{12}$$

where the specific heat capacity of the nanofluid $C_{p_{nf}}$ is determined by the volumetric concentration ϕ_{np} of the nanoparticle as well as the specific heat capacity of the base fluid $C_{p_{bf}}$ and the nanoparticle $C_{p_{np}}$ [15]. Xuan and Roetzel [41] extended the approach of Pak and Cho [15] by considering the density ρ and applying the mixture rule to mass per cent, and, therefore, the specific heat capacity is calculated as follows:

$$C_{p_{nf}} = \frac{\phi_{np} \times \rho_{np} \times C_{p_{np}} + \left(1 - \phi_{np}\right) \times \rho_{bf} \times C_{p_{bf}}}{\rho_{nf}}. \tag{13}$$

Based on measurements of Al_2O_3 and ZnO in EG/W (60/40), and SiO_2 in W, Vajjha and Das [20] developed a correlation that is related to a temperature range of 315 to 363 K

and a volumetric concentration range of 0 to 0.1 for Al_2O_3 and SiO_2 and 0 to 0.07 for ZnO nanofluids, and the specific heat capacity can be calculated according to

$$C_{p_{nf}} = \frac{A_V \times T + B_V \times \left(\frac{C_{p_s}}{C_{p_{bf}}}\right)}{C_V + \varphi_{np}} \times C_{p_{bf}}. \quad (14)$$

Here, the coefficients A_V, B_V, and C_V are empirical parameters, which are adapted to the measurement data for the respective nanofluids. Table 2 provides a summary of the parameters for the nanofluids Al_2O_3, ZnO in EG/W (60/40), and SiO_2 in W.

Table 2. Empirical parameter for Vajjha and Das [20] correlation for different nanofluids of Equation (14).

Nanofluid	Base Fluid	A_V	B_V	C_V
Al_2O_3	EG/W (60/40)	0.0008911	0.5179	0.4250
ZnO	EG/W (60/40)	0.0004604	0.9855	0.2990
SiO_2	W	0.0017690	1.1937	0.8021

3.3. Thermal Conductivity

For thermal conductivity, various correlations can be found in literature due to its importance for heat transfer. The models for thermal conductivity differ in terms of the number and type of dependencies like temperature, pressure, and concentration as well as empirical parameters, and nanoparticle sizes, and shapes [8,16,42]. Measurement data from different authors vary widely due to different measurement methods and different concentrations of the nanoparticles in the base fluid, with enhancements ranging from 14 to 250% [28]. Therefore, the experimental data sets for the thermal diffusivity and thermal conductivity are compared with correlations suitable for SiO_2 nanofluids.

In the literature, Maxwell's correlation is often used to determine thermal conductivity, as it offers a simple approach. To apply the Maxwell correlation, only the thermal conductivities of the two substances involved and their concentration are required. However, the thermal interactions between the filler particles are neglected, which is why this correlation is only valid for low particle concentrations below 25 vol.% [43] The Bruggeman theory follows a similar approach, but also remains applicable for higher particle concentrations, as it takes into account the interactions between the particles with increasing numbers. Despite this extended validity, the Bruggeman correlation is used less frequently than the Maxwell correlation in the literature on nanofluids. In most real applications, low concentrations of nanoparticles are used; therefore, this study focuses on Maxwell's correlation. In the Maxwell correlation, the thermal conductivity

$$k = k_{bf} \frac{k_{np} + 2k_{bf} - 2(k_{bf} - k_{np})\phi}{k_{np} + 2k_{bf} + (k_{bf} - k_{np})\phi} \quad (15)$$

of SiO_2-based nanofluids is calculated with the assumption of perfect spherical nanoparticles [44]. For this reason, Hamilton and Crosser [45] proposed a further approach, which extended the correlation of Maxwell et al. [44] by taking particle sphericity into account, and then the thermal conductivity can be calculated according to

$$k = k_{bf} \frac{k_s + (ß - 1)k_{bf} - (ß - 1)(k_{bf} - k_s)\phi}{k_s + (ß - 1)k_{bf} + (k_{bf} - k_s)\phi} \quad (16)$$

where the shape factor ß equals $3/\psi$. Particle sphericity, denoted as ψ, is the ratio of the sphere's surface area with the same volume as the particle to the surface area of the particle itself. It ranges from 0 to 1, where 1 means perfectly spherical.

Specifically, for SiO_2 nanofluids, Rejvani et al. [28] developed a temperature- and concentration-based correlation defined as follows:

$$k = 0.53235 + 3.19365 \times 10^{-3} T + 0.75868\phi - 1.73673 \times 10^{-5} T^2. \quad (17)$$

The concentration ranges from 0 to 1.5 wt.% with a temperature range from 298 to 323 K.

3.4. New Empirical Correlation for Density, Specific Heat Capacity, and Thermal Diffusivity

None of these state-of-the-art correlations can output the value of the properties as a function of both the concentration and the temperature up to a concentration of 20 wt.%. Therefore, a new empirical correlation for SiO_2 nanoparticles in base fluid is developed. It is valid for all three thermophysical properties (TPP), $\rho(T, \varphi)$, $c_p(T, \varphi)$, and $a(T, \varphi)$, for a temperature range of 293.15 to 323.15 K and a mass concentration range of SiO_2 nanoparticles in the base fluid water and ethylene glycol/water mixture (25/75) of 0 to 20 wt.%, and is defined as

$$TPP(T, \phi) = TPP(T, 0) \times \left(1 + \mathrm{A} \times \mathrm{T} \times \phi^B\right) \quad (18)$$

with A in 1/K and B being adjustable parameters. The structure of the correlation is selected based on the property of the base fluid to eliminate large deviations at low concentrations. Only the mass concentration ϕ and the temperature T in K, as well as the value of the base fluid, are required. Both parameters A and B are adapted for each property and base fluid and compared with the obtained measurement data and the other correlations from the literature.

3.5. Validation

For the validation of the experimental data for the pure base fluids, the measurement data are compared with the calculated values from REFPROP v.10.0 and the reported data from the literature [35].

The relative deviation (RD) between the experimental (exp), literature, and calculated (calc) data is determined by

$$\mathrm{RD} = \frac{\left|z_{\mathrm{exp}} - z_{\mathrm{calc}}\right|}{z_{\mathrm{exp}}} \times 100\% \quad (19)$$

and the root mean square error (RMSE) is defined as

$$\mathrm{RMSE} = \sqrt{\frac{1}{\mathrm{n}} \sum_{\mathrm{i}=1}^{\mathrm{n}} \left(z_{\mathrm{exp},i} - z_{\mathrm{calc},i}\right)}. \quad (20)$$

Due to the limitations of the data available for certain concentrations and temperature ranges for SiO_2 nanofluids, the results are compared with the shown correlations from Section 3.

4. Results

In this chapter, the results of the properties of transmission, density, specific heat capacity, and thermal diffusivity for the pure components water and water–ethylene glycol are first compared with the literature, and then the results of the measurements of the same properties with nanofluids are discussed.

4.1. Pure Components

The measured transmission of the pure fluids water and ethylene glycol over a wavelength range of 300 to 1700 nm is shown in Figure 8. The results of the two spectrometers are

in very good agreement with the literature values for water obtained by Otanicar et al. [31] and Karami et al. [46] with deviations smaller than 0.6%.

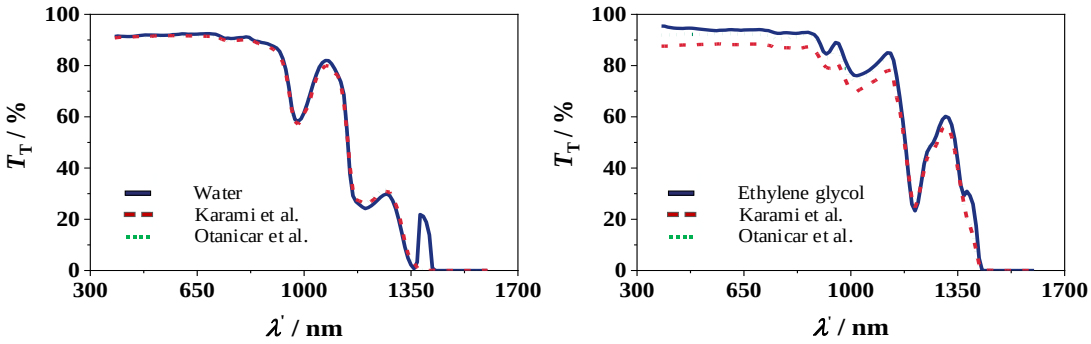

Figure 8. Transmission of water (**left**) and ethylene glycol (**right**), redrawn based on Otanicar et al. [31] and Karami et al. [46].

For ethylene glycol, the measurements are in good agreement with the literature value obtained by Otanicar et al. [31] with deviations of 2%, while there are deviations of 7% compared to the values obtained by Karami et al. [46].

The thermophysical properties density, specific heat capacity, and thermal diffusivity are shown as a function of the temperature of water and the ethylene glycol/water mixture in Figure 9. Each measurement is compared with calculated values from REFPROP [35] and experimental data from the literature. The results of the water density measurements are compared with those of Sharma et al. [47], Shi et al. [48], Moosave and Rostami [49], and Arnautovic et al. [50]. In addition to REFPROP [35], data from Moosave and Rostami [49] are used to validate the density of ethylene glycol. The deviations of the measurement data and all literature values for water and ethylene glycol are within 1% in comparison to REFPROP [35]. The specific heat capacities of water and ethylene glycol are validated with experimental data from Nan et al. [51]. This experimental data are in good agreement with REFPROP [35] within a deviation of 5%. The thermal diffusivity of water and ethylene glycol is compared against the literature data and REFPROP [35]. The water measurements are validated with data from Zhang et al. [52], and, for ethylene glycol, with data from Balderas and Lopez et al. [53] and Eckert and Drake [54]. This results in a maximum relative deviation of 6% compared to REFPROP [35].

4.2. Nanofluid

The measurements of the thermophysical properties are carried out for SiO_2 nanoparticles in W and EG/W (25/75). In contrast to the pure fluids, there are only a few experimental data available for the thermophysical properties of SiO_2 nanofluids. For verification, the experimental data are compared to the published data. If this is not possible, the measured data are compared with the correlations shown in Section 3. In addition, adjustable parameters for Equation (18) are developed from the experimental data.

4.2.1. Sample Stability

In order to verify the long-term stability of the dispersions, absorbance measurements were first carried out for selected concentrations (1 wt.%, 10 wt.%, and 20 wt.%) over a period of 7 days using FT-IR. A quantification calculation was performed for several freshly dispersed concentrations. Each measurement on subsequent days was quantified using this method to assess the concentrations of the fluids. It is found that the absorbance bands deviated by less than 0.4 wt.% from the original measurement over this period. The calculation is carried out over the entire wavenumber range of 200 to 4000 cm^{-1}. The characteristic peak for SiO_2 at 1120 cm^{-1} can be seen in detail in Figure 10. Here, it can also be observed that there is no significant change in any of the three concentrations over the period of 7 days.

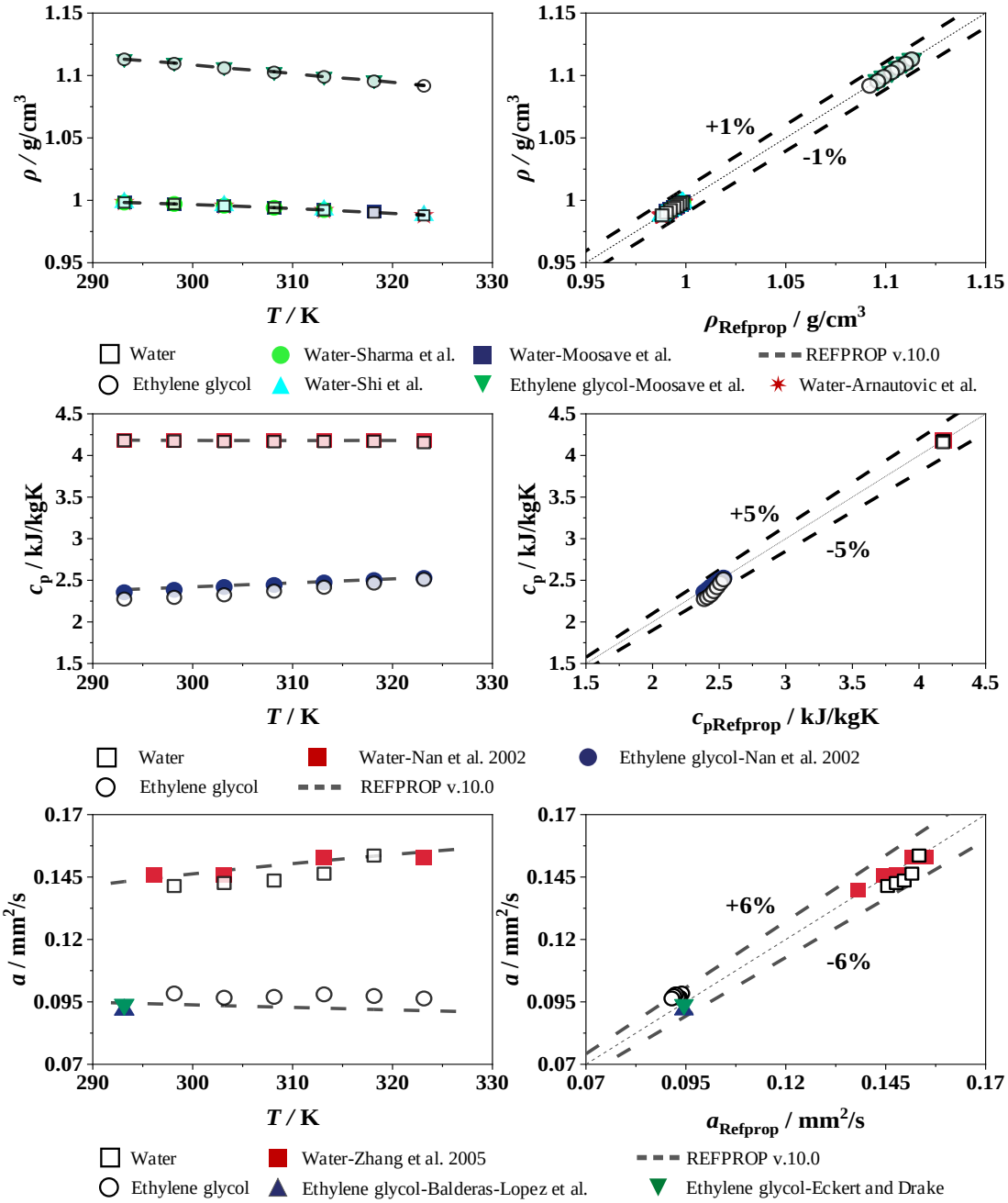

Figure 9. Density, specific heat capacity, and thermal diffusivity (**left**), and deviation (**right**) of the pure components water and ethylene glycol; redrawn based on Sharma et al. [47], Shi et al. [48], Moosave and Rostami [49], Arnautovic et al. [50], Nan et al. [51], Zhang et al. [52], Balderas-Lopez et al. [53] and Eckert and Drake [54].

In comparison to the literature, Mukherjee et al., for example, had a deviation in the zeta potential of 5% over the same period [29]. Ferrouillat et al. were able to demonstrate a deviation from the initially measured 34 wt.% to 31 wt.% after 14 days, whereby, here, the stability was only assessed using the measurement results [26]. It can, therefore, be concluded that the dispersions used in this study are stable for a minimum of seven days, and, thus, are unlikely to influence the results of the measurements taken.

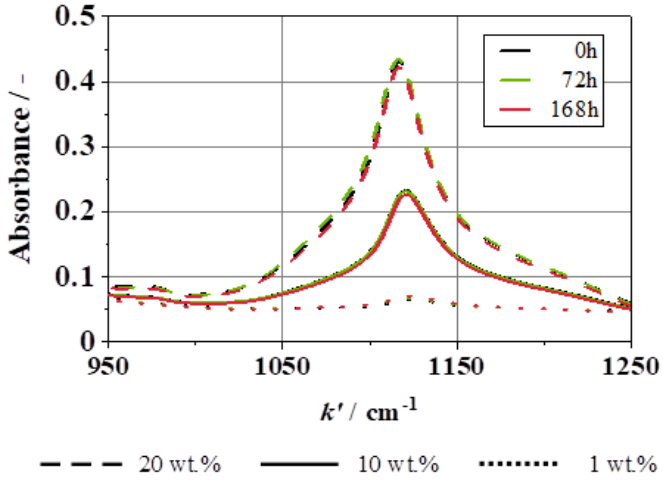

Figure 10. Absorbance spectra of SiO_2 particles dispersed in water, 1 wt.%, 10 wt.%, and 20 wt.% directly after dispersion, 72 h later, and 168 h later.

4.2.2. Transmission

Figure 11 shows the measured transmission, and absorption coefficients calculated using Equation (2) for the different nanoparticle concentrations over the wavelength. On the left-hand side, the transmission and absorption for W are plotted, while, on the right-hand side, the transmission and absorption for EG/W (25/75) are shown. Due to the low transmission in the higher wavelength range and the resulting large absorption coefficients, the *y*-axis of the absorption coefficients is adjusted for detectability. When comparing the addition of nanoparticles to the different base fluids, water, and the ethylene glycol/water mixture, there are almost no differences. A decrease in transmission in the visible range of the spectrum from 380 to 800 nm can be observed as the concentration of nanoparticles increases in both base fluids, which leads to a decline in the transmission of 9.3% at 20 wt.% SiO_2 nanofluid compared to the respective base fluid.

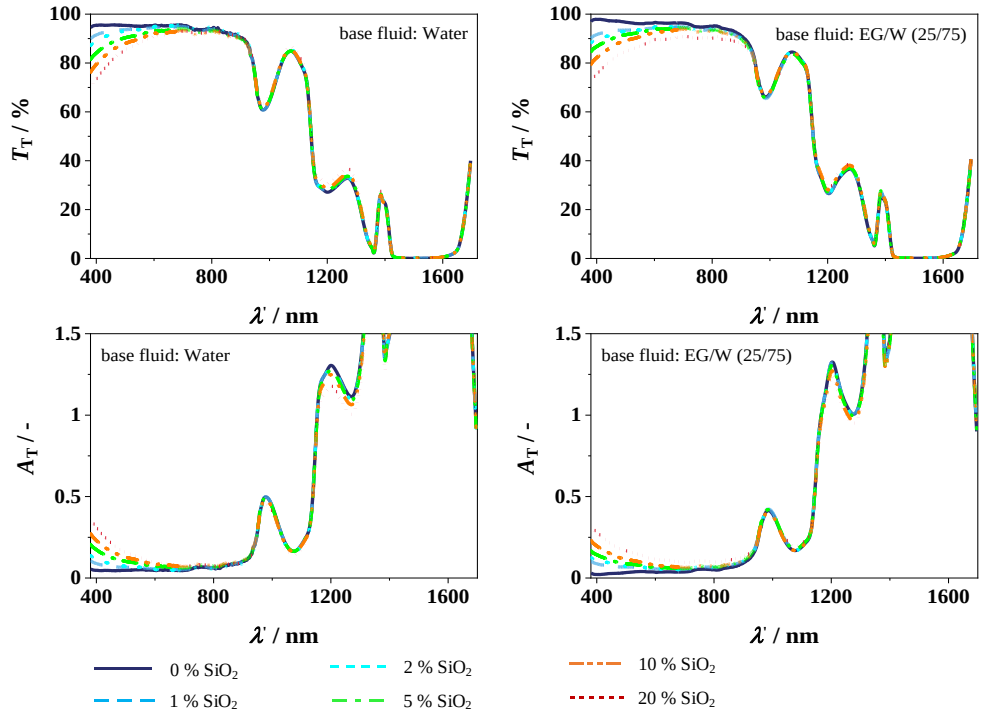

Figure 11. Transmission (**top**) and absorption coefficient (**bottom**) of SiO_2 in W (**left**) and EG/W (25/75) (**right**).

From the beginning of the infrared range at a wavelength of about 800 nm, there is almost no change in transmission to the base fluids with the addition of nanoparticles. With the increasing nanoparticle content, the transmission in the infrared range is slightly higher, with up to 1.2% for 20 wt.% SiO_2 in W, while, for 20 wt.% SiO_2 in EG/W (25/75), the transmission is 2.8% lower compared to the base fluid. But this can be neglected when considering the entire wavelength range of 380 to 1700 nm. Overall, the absorption is slightly increased with the addition of SiO_2 nanoparticles, with a maximum at 20 wt.% SiO_2 of 4.7% compared to W and up to 11.7% compared to EG/W. This results in a lower transmission in the visible range.

The addition of SiO_2 nanoparticles results in additional absorption bands within the fluid. Furthermore, the particles also lead to an increased scattering, which, consequently, results in an increased effective path length of the light in the material. Overall, this results in an increased absorption by the nanoparticles, which is particularly evident in the visible range. However, due to the already pronounced absorption of water and ethylene glycol in the infrared range, this effect is less pronounced there.

4.2.3. Density

Figures 12 and 13 show the experimental results for the density of SiO_2 in W and EG/W (25/75), with concentrations from 0 to 20 wt.% over a temperature range of 293 to 323 K. The adjustable parameters of SiO_2 in W and EG/W (25/75) for Equation (18) are shown in Table 3 and will be compared to the correlation of Pak and Cho [15].

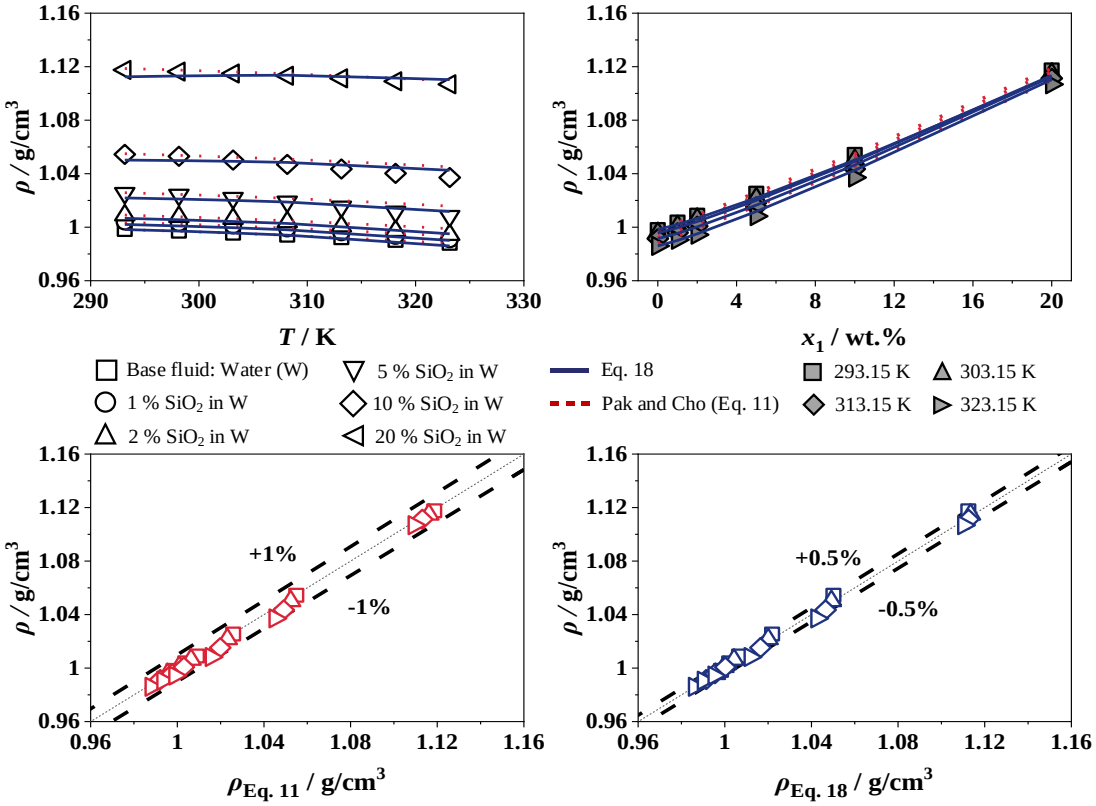

Figure 12. Density of SiO_2 in water (**top**) and deviation to Equation (11) (**left**) and to Equation (18) (**right**); Pak and Cho [15].

The addition of nanoparticles does not change the temperature dependence of the density. At a constant concentration, the density decreases with rising temperature, while, at a constant temperature, the density increases linearly with increasing SiO_2 concentration up to 12.3% and 11.3% compared to the base fluids W and EG/W (25/75), respectively, which is expected due to the higher density of SiO_2.

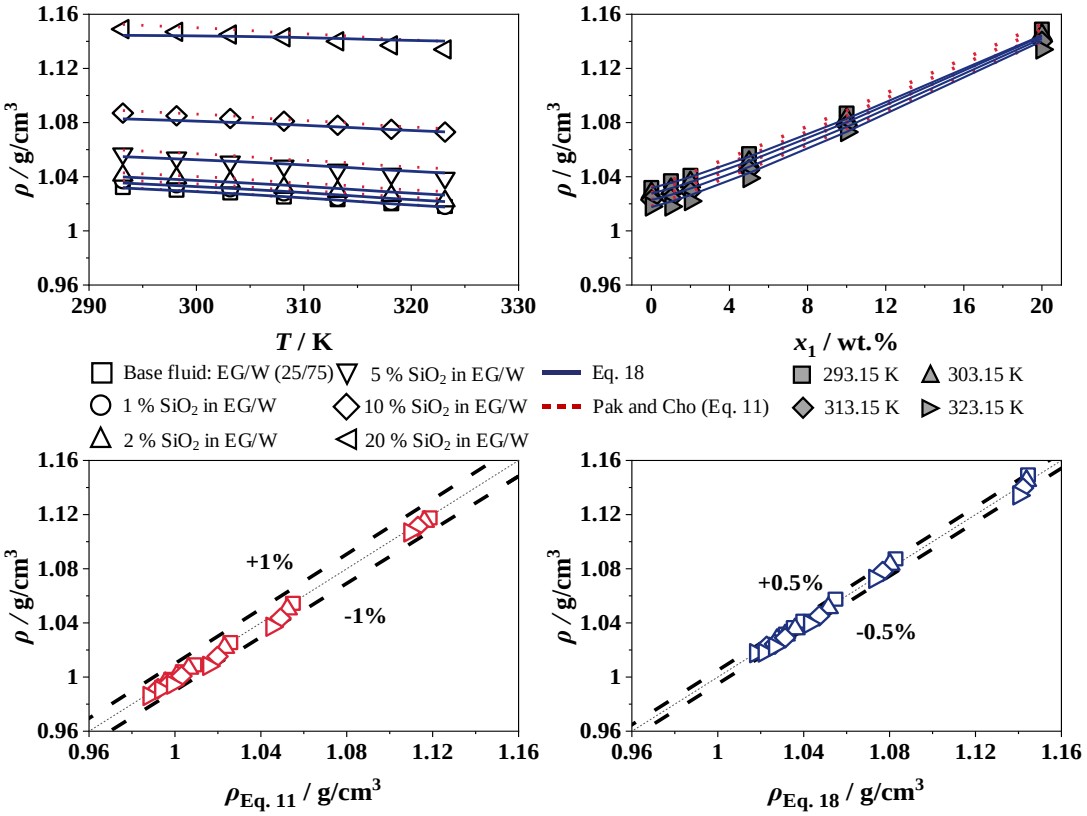

Figure 13. Density of SiO_2 in EG/W (25/75) (**top**) and deviation to Equation (11) (**left**) and to Equation (18) (**right**), Pak and Cho [15].

Table 3. Adjustable parameters of Equation (18) for the density of SiO_2 in W and EG/W (25/75).

	Density		
	A	B	RSME
base fluid water	0.002432	1.137	0.002297
base fluid EG/W (25/75)	0.002346	1.143	0.002361

The maximum error of the measurement is 0.00015 g/cm^3, which is significantly less than the system's measurement accuracy. The correlations show very good agreement with relative deviations of less than 1% for Pak and Cho [15] and 0.5% for Equation (18) for SiO_2 in W and EG/W (25/75). Table 4 show the experimental values for the density of SiO_2 in W and EG/W (25/75), with concentrations from 0 to 20 wt.% over a temperature range of 293 to 323 K.

4.2.4. Specific Heat Capacity

The experimental results for the specific heat capacity of SiO_2 in W and EG/W (25/75) are shown in Figures 14 and 15 with concentrations from 0 to 20 wt.% over a temperature range of 293 to 323 K. The maximum error of the measurement is 2%, which is less than the measurement accuracy of the system. The experimental data are compared with the correlations from Pak and Cho [15], Xuan and Roetzel [41], and Vajjha and Das [20], as well as Equation (18). The adjustable parameters for SiO_2 in W and EG/W (25/75) for Equation (18) are shown in Table 5.

Table 4. Experimental density of SiO_2 in W and EG/W (25/75) at 100 kPa [a].

Base Fluid	**Water**					
SiO_2 (wt.%)	**0**	**1**	**2**	**5**	**10**	**20**
Temperature K	**Density g/cm^3**	**g/cm^3**	**g/cm^3**	**g/cm^3**	**g/cm^3**	**g/cm^3**
293.15	0.99827	1.00388	1.00898	1.02541	1.05442	1.11754
298.15	0.99710	1.00267	1.00783	1.02415	1.05297	1.11633
303.15	0.99569	1.00093	1.00638	1.02178	1.05018	1.11488
308.15	0.99408	0.99867	1.00389	1.01900	1.04691	1.11320
313.15	0.99143	0.99580	1.00073	1.01523	1.04349	1.11126
318.15	0.98875	0.99313	0.99734	1.01147	1.04028	1.10909
323.15	0.98602	0.99058	0.99436	1.00822	1.03710	1.10681
Base fluid	**EG/W (25/75)**					
SiO_2 (wt.%)	**0**	**1**	**2**	**5**	**10**	**20**
Temperature K	**Density g/cm^3**	**g/cm^3**	**g/cm^3**	**g/cm^3**	**g/cm^3**	**g/cm^3**
293.15	1.03170	1.03652	1.04126	1.05747	1.08731	1.14934
298.15	1.02974	1.03391	1.03855	1.05403	1.08530	1.14733
303.15	1.02763	1.03093	1.03551	1.05115	1.08313	1.14509
308.15	1.02534	1.02754	1.03200	1.04824	1.08076	1.14250
313.15	1.02275	1.02431	1.02897	1.04517	1.07803	1.13970
318.15	1.02001	1.02111	1.02568	1.04209	1.07527	1.13694
323.15	1.01762	1.01805	1.02239	1.03927	1.07252	1.13416

[a] Uncertainties u : $u_{DMA}(T) = 0.03$ K, $u_r(\rho) = 0.003$ g/cm^3, and $u_{scale}(wt) = 0.0167$ wt.%.

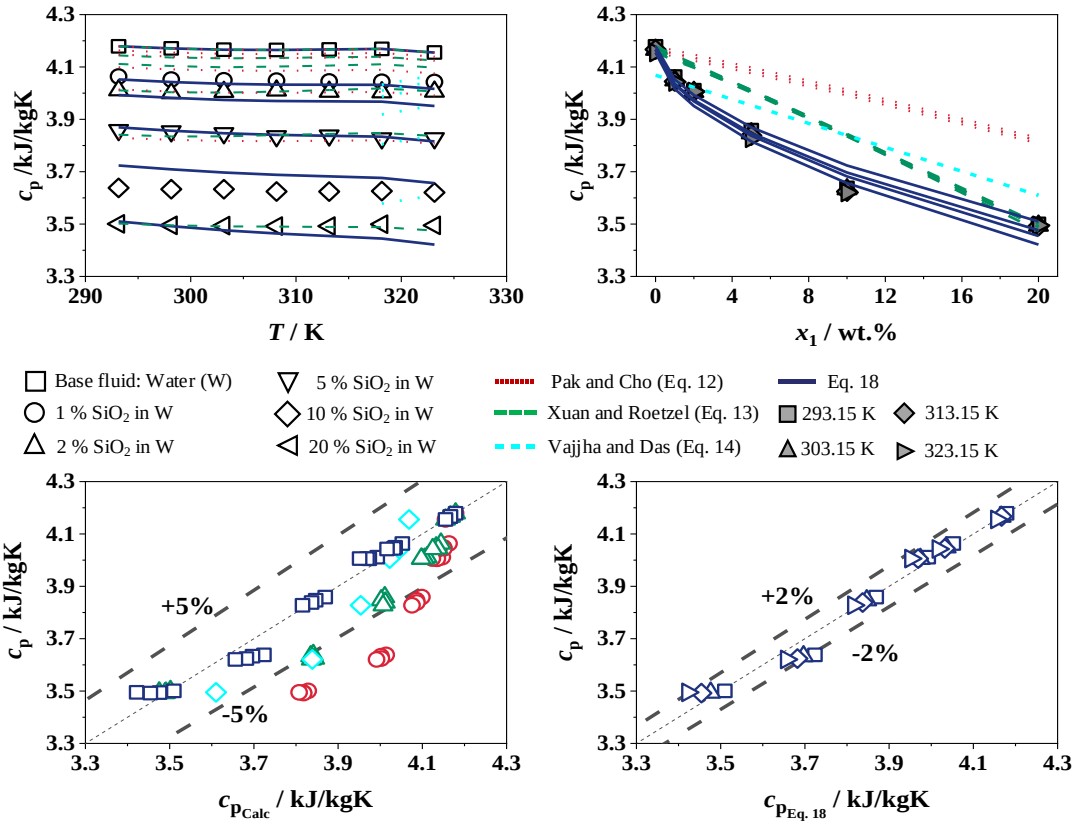

Figure 14. Specific heat capacity of SiO_2 in W (**top**) and deviation to Equations (12)–(14) (**left**) and Equation (18) (**right**), Pak and Cho [15] in red, Xuan and Roetzel [41] in green, and Vajjha and Das [20] in turquoise.

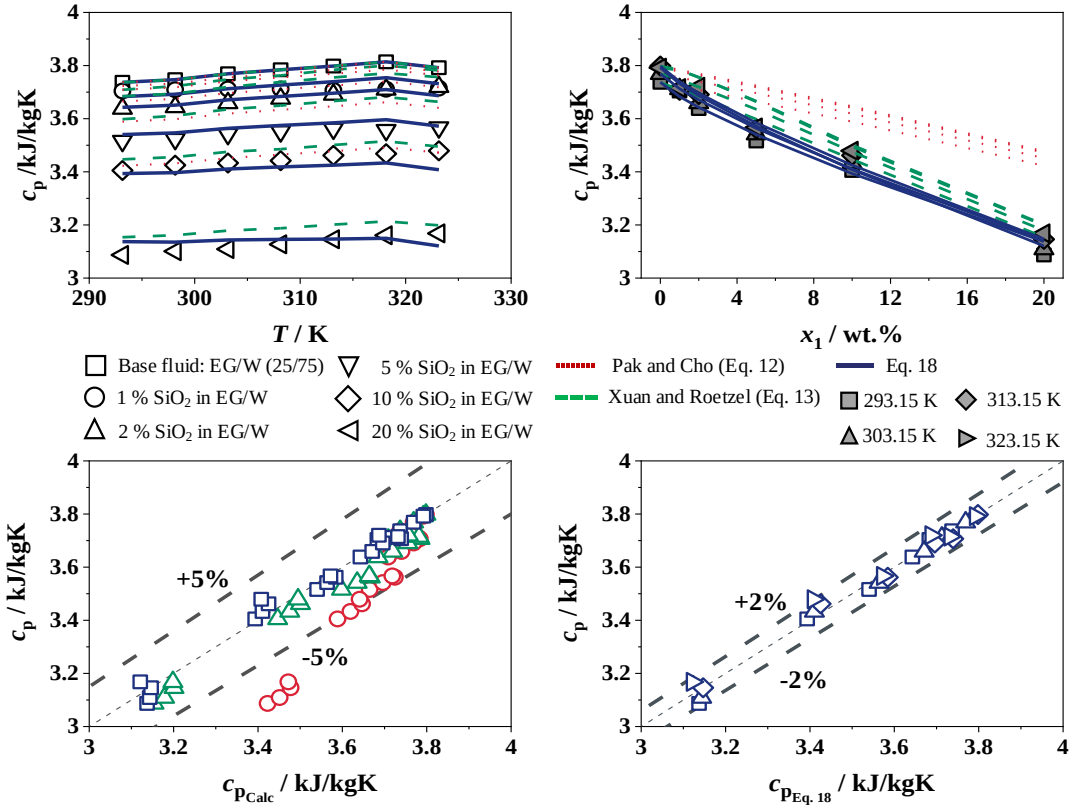

Figure 15. Specific heat capacity of SiO_2 in EG/W (25/75) (**top**) and deviation to Equations (12) and (13) (**left**) and to Equation (18) (**right**), Pak and Cho [15] in red, Xuan and Roetzel [41] in green.

Table 5. Adjustable parameters of Equation (18) for the specific heat capacity of SiO_2 in W and EG/W (25/75).

	Specific Heat Capacity		
	A	B	RMSE
base fluid water	−0.00134	0.5558	0.008291
base fluid EG/W (25/75)	−0.00200	0.8043	0.006693

With the increase in SiO_2, the temperature dependence of the measured specific heat capacity behaves like the base fluids. For the water-based nanofluid, the measured specific heat capacity shows a maximum decrease of 0.5% between 293 to 323 K, while the calculated values from Vajjha and Das [20] are more temperature-dependent and show a small increase in the specific heat capacity of about 0.6% from 318 to 323 K. As with the experimental data, the correlations from Pak and Cho [15] and Xuan and Roetzel [41] show a slightly decreasing specific heat capacity with increasing temperature at a constant concentration of SiO_2 in W. At a constant temperature and with an increasing concentration of SiO_2, the specific heat capacity decreases by up to 7.7% at an SiO_2 concentration of 5 wt.%, after which the decrease flattens out to a 15.9% lower specific heat capacity at 20 wt.% compared to the pure W. The correlations of Pak and Cho [15] and Xuan and Roetzel [41] show decreasing specific heat capacity curves, which do not reproduce the course of the measured data. The correlation of Pak and Cho [15] deviates by more than 5% for concentrations of 5 to 20 wt.% SiO_2 in W compared with the experimental data. Likewise, the correlation of Xuan and Roetzel [41] reveals deviations of up to 5% at 10 wt.% and only meets the experimental results at a mass fraction of 20 wt.% of SiO_2 in W. The deviations of the correlations from the literature occur regardless of whether a general model such as Pak and Cho [15] and Xuan and Roetzel [41] or a model specific to the SiO_2 nanofluid by Vajjha and Das [20] is applied.

When interpreting the measurement data and the described deviations from the models, it must be considered that the nanoparticles are quite small with an average diameter of 28 nm, which increases the surface area compared to nanoparticles with a larger diameter. Zhang et al. [55] confirmed this with specific heat capacity measurements with different particle sizes of SiO_2 and concluded that the specific heat capacity is lower with smaller particles. Similarly, the strong decrease is supported by measurements with different nanofluids by O'Hanley et al. [17], who measured up to 5% lower heat capacities for Al_2O_3 in water in the range of up to 10 wt.% compared to Equation (14). A comparison of the measurements by Pantzali et al. [56] also shows a lower heat capacity for CuO particles in water of 1 to 6%. In contrast to the other correlations, the measured data can be predicted very well using Equation (18) with the parameters developed in Table 5 with a maximum relative deviation of less than 2%. The experimental values for the specific heat capacity of SiO_2 in W and EG/W (25/75) are shown in Table 6, with concentrations from 0 to 20 wt.% over a temperature range of 293 to 323 K.

Table 6. Experimental specific heat capacity of SiO_2 in W and EG/W at 100 kPa [a].

Base Fluid	**Water**					
SiO_2 (wt.%)	**0**	**1**	**2**	**5**	**10**	**20**
Temperature	**Specific heat capacity**					
K	**kJ/kgK**	**kJ/kgK**	**kJ/kgK**	**kJ/kgK**	**kJ/kgK**	**kJ/kgK**
293.15	4.179	4.064	4.011	3.859	3.638	3.501
298.15	4.171	4.052	4.000	3.854	3.633	3.495
303.15	4.166	4.049	4.005	3.847	3.633	3.494
308.15	4.165	4.048	4.010	3.835	3.625	3.492
313.15	4.167	4.045	4.006	3.838	3.624	3.492
318.15	4.169	4.043	4.003	3.827	3.626	3.499
323.15	4.155	4.043	4.006	3.828	3.621	3.495
Base fluid	**EG/W (25/75)**					
SiO_2 (wt.%)	**0**	**1**	**2**	**5**	**10**	**20**
Temperature	**Specific heat capacity**					
K	**kJ/kgK**	**kJ/kgK**	**kJ/kgK**	**kJ/kgK**	**kJ/kgK**	**kJ/kgK**
293.15	3.737	3.704	3.638	3.516	3.405	3.087
298.15	3.747	3.709	3.644	3.523	3.425	3.101
303.15	3.769	3.712	3.659	3.542	3.433	3.109
308.15	3.784	3.712	3.676	3.552	3.442	3.127
313.15	3.798	3.707	3.691	3.562	3.462	3.146
318.15	3.814	3.711	3.710	3.557	3.468	3.161
323.15	3.792	3.715	3.721	3.567	3.479	3.168

[a] Uncertainties u : $u_{DSC}(T) = 0.1\ K$, $u_r(c_p) = 0.03$, and $u_{scale}(wt) = 0.0167$ wt.%.

For the SiO_2 nanofluid with EG/W as the base fluid and a constant concentration, the specific heat capacity rises with increasing temperature to a maximum of 2.3% at 323 K for 2 wt.% SiO_2 in EG/W (25/75). This is due to the addition of ethylene glycol, which has a higher capacity than pure water with increasing temperature. Furthermore, the specific heat capacity decreases with an increasing nanoparticle concentration for SiO_2 in EG/W (25/75) at a constant temperature of up to 17.3% compared to the base fluid. The correlations of Pak and Cho [15] and Xuan and Roetzel [41] predict greater specific heat capacities when nanoparticles are added to the ethylene glycol/water mixture, resulting in relative deviations of up to 5%. As with the base fluid water, Equation (18) agrees well with the SiO_2 in EG/W (25/75) with a maximum relative deviation of up to 2%.

4.2.5. Thermal Diffusivity and Conductivity

The thermal diffusivity of SiO_2 in W and EG/W (25/75) is shown in Figure 16. The mean standard deviation of the measured thermal diffusivity is 3.3%. For pure water,

the thermal diffusivity is temperature-dependent from 298 to 323 K, increasing by 8.6%, which remains with the addition of SiO_2 nanoparticles. For a constant temperature, the thermal diffusivity increases with a higher nanoparticle concentration up to a maximum of 16.4% at 20 wt.%. This is to be expected, as the thermal diffusivity of the pure SiO_2 is significantly higher than the base fluid. In addition, the thermal diffusivity increases with rising temperature. The adjustable parameters for Equation (18) are shown in Table 7.

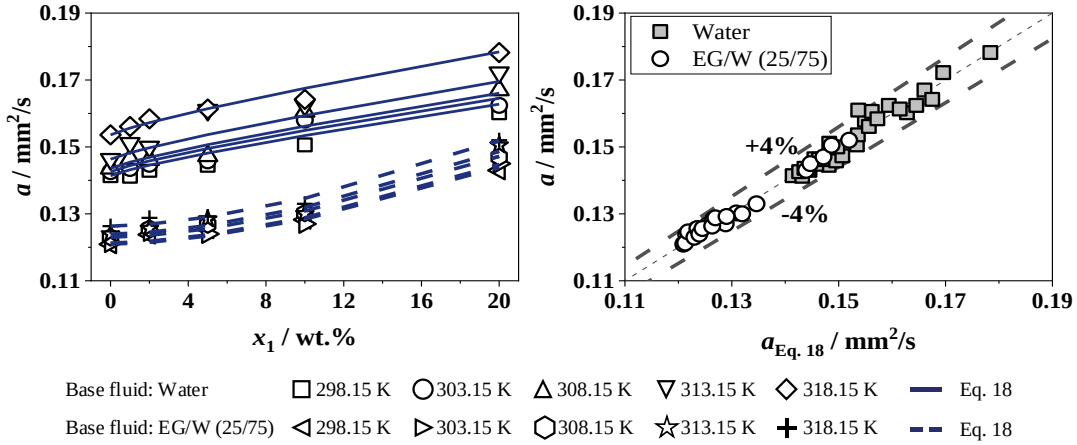

Figure 16. Thermal diffusivity of SiO_2 in W and in EG/W (25/75) (**left**) and deviation to Equation (18) (**right**).

Table 7. Adjustable parameters of Equation (18) for the thermal diffusivity of SiO_2 in W and EG/W (25/75).

	Thermal Diffusivity		
	A	B	RMSE
base fluid water	0.001936	0.8322	0.01725
base fluid EG/W (25/75)	0.008746	1.6270	0.011038

The thermal diffusivity of EG/W (25/75) is also temperature-dependent from 298 to 318 K but with a smaller incline of 4.5%. With the addition of SiO_2 nanoparticles, the temperature dependence of the thermal diffusivity of the fluid is similar. With a constant temperature, SiO_2 in EG/W has a significantly greater rise of up to 20.4%, both at the highest concentration and temperature measured. Furthermore, Equation (18) is compared with the experimental data and shows a maximum relative deviation of less than 4% with temperatures of 298 to 318 K over a concentration range of 0 to 20 wt.%.

With the additional measurement of the density and specific heat capacity (see Sections 4.2.2 and 4.2.3), the thermal conductivity can be determined by Equation (10). This is visualized in Figure 17 for the nanofluids W and EG/W as a function of SiO_2. The values of the thermal diffusivity of SiO_2 in W and EG/W (25/75) is shown in Table 8.

The experimental data with the base fluid W are compared with data from Ferrouillat et al. [26] and Mukherjee et al. [29], as well as Rejvani et al. [28], and is additionally compared with calculated values from Equation (18). Figure 1 shows that the nanoparticles are almost spherical. However, the exact sphericity cannot be calculated. Therefore, the correlation of Hamilton and Crosser [45] will not be considered further and only the correlation of Maxwell [44] will be discussed in this work. The thermal conductivity of SiO_2 in W determined from the measured results shows a decrease of 3% up to a concentration of 5 wt.%. With a higher concentration of SiO_2 nanoparticles, the expected increase in thermal conductivity can be seen with a maximum of 9% compared to the base fluid at 20 wt.%. The increase in thermal conductivity is due to the movement of nanoparticles, which allows energy to migrate to physical locations (i.e., transfer from one place to another). The strength of these movements affects the thermal conductivity coefficient. Furthermore, the thermal

conductivity of SiO_2 nanoparticles is higher than that of the base fluid, which results in an enhanced overall heat flow within the fluid [55]. The effect of the interfacial layer must also be considered for thermal conductivity. The thickness of this layer is typically a few nanometers and has a different thermal conductivity to the particle and the base fluid. This can have a positive effect on the thermal conductivity of the nanofluid, with the thermal conductivity of the particle being higher than that of the base fluid [57]. Regarding the particle size, the thermal conductivity gradually increases as the radius of the particles decreases. Nanoparticles of a smaller size are more active in Brownian motion and heat transport than larger particles [55]. Therefore, the coefficient of thermal conductivity increases with decreasing particle size. In summary, smaller nanoparticles allow better heat transfer than larger particles due to their more intense motion [55].

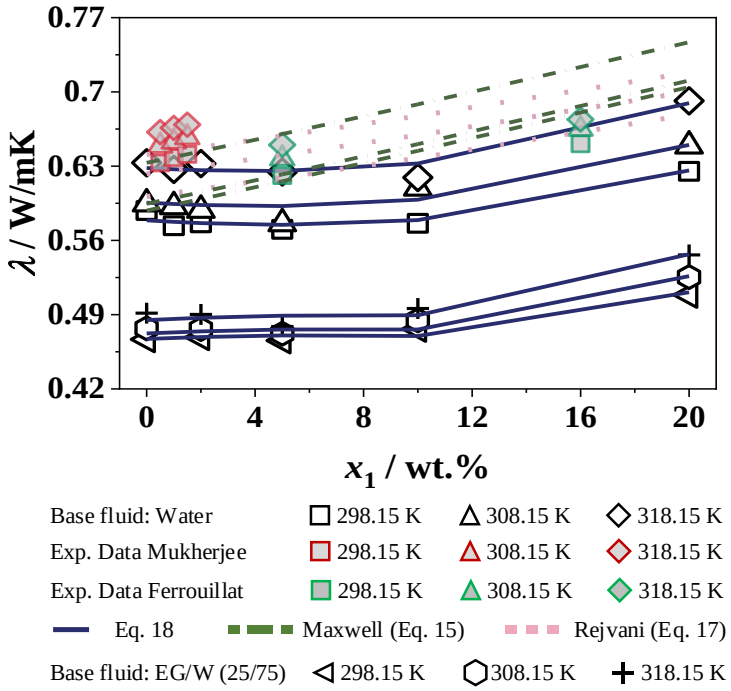

Figure 17. Thermal conductivity of SiO_2 in W and in EG/W (25/75), Maxwell et al. [44] and Rejvani et al. [28].

Compared to the measurement data, the data from Mukherjee et al. [29], which are measured from the sound velocities applying a modified Bridgman equation [58], show a constant increase in the low concentration range of up to 3 wt.%. Ferrouillat et al. [26], who used a flow loop with a horizontal tube test section with steady-state measurement methods to investigate the thermal conductivity, provide no experimental data in the concentration range up to 5 wt.%, after which an increase in thermal conductivity can also be seen. The calculated values with the correlations by Maxwell et al. [44] and Rejvani et al. [28] show a constant increase in thermal conductivity with increasing concentration, while at the maximum concentration of 20 wt.%. Maxwell et al. [44] provide a higher enhancement of 20% compared to the base fluid and an increase of 12% could be obtained with the correlation by Rejvani et al. [28].

The same applies to the nanofluid concentration in EG/W. In the base fluid EG/W (25/75), the thermal conductivity is also temperature-dependent with an increase of 5% at a temperature of 318 K. This does not change with the addition of SiO_2 nanoparticles. At a constant temperature, the thermal conductivity decreases slightly by 1% up to a mass fraction of 5 wt.%. It subsequently increases by up to 12% compared to the base fluid at the highest SiO_2 concentration.

Table 8. Experimental thermal diffusivity of SiO_2 in W and EG/W at 100 kPa [a].

Base Fluid	**Water**					
SiO_2 (wt.%)	**0**	**1**	**2**	**5**	**10**	**20**
Temperature	**Thermal Diffusivity**					
K	**mm^2/s**	**mm^2/s**	**mm^2/s**	**mm^2/s**	**mm^2/s**	**mm^2/s**
298.15	0.1414	0.1412	0.1431	0.1445	0.1506	0.1602
303.15	0.1427	0.1436	0.1448	0.1458	0.1580	0.1624
308.15	0.1436	0.1464	0.1462	0.1473	0.1606	0.1670
313.15	0.1463	0.1511	0.1500	0.1610	0.1624	0.1722
318.15	0.1536	0.1561	0.1584	0.1613	0.1642	0.1782
Base fluid	**Ethylene glycol/Water (25/75)**					
SiO_2 (wt.%)	**0**	**2**	**5**	**10**	**20**	
Temperature	**Thermal Diffusivity**					
K	**mm^2/s**	**mm^2/s**	**mm^2/s**	**mm^2/s**	**mm^2/s**	
298.15	0.1209	0.1238	0.1254	0.1283	0.1433	
303.15	0.1213	0.1246	0.1240	0.1271	0.1452	
308.15	0.1230	0.1256	0.1268	0.1303	0.1469	
313.15	0.1239	0.1256	0.1284	0.1324	0.1505	
318.15	0.1263	0.1288	0.1292	0.1330	0.1521	

[a] Uncertainties u : $u_{LFA}(T) = 0.1\ K$, $u_r(a) = 0.05$, and $u_{scale}(wt) = 0.0167$ wt.%.

5. Conclusions

The thermophysical measurements of SiO_2 nanoparticles (0, 1, 2, 5, 10, and 20 wt.%) in pure water (W) and an ethylene glycol–water mixture (EG/W) in a weight ratio of 25/75 from 298 to 323 K at 100 kPa are performed with a density meter, differential scanning calorimetry, and a laser flash method with validation measurements on the respective pure fluids. The results are compared with experimental data and with correlations from the literature. The maximum relative deviations of the pure fluids W and EG/W compared to REFPROP [35] are less than 1% for the density, less than 5% for the specific heat capacity, and less than 6% for the thermal diffusivity. By producing different concentrations of nanofluid, a correlation is established for each of the thermophysical properties based on the experimental results.

- At a constant concentration, the density decreases with increasing temperature, while, at constant temperature, the density increases linearly with an increasing SiO_2 concentration of up to 12.3% and 11.3% compared to the base fluids W and EG/W (25/75), respectively.
- At a constant temperature and with an increasing concentration of SiO_2 in W, the specific heat capacity decreases strongly by up to 7.7% at 5 wt.% SiO_2, after which the decrease flattens out to a 15.9% lower specific heat capacity at 20 wt.% compared to pure W. For SiO_2 in EG/W (25/75), the specific heat capacity decreases with an increasing nanoparticle concentration at a constant temperature by up to 17.3%. The correlations of Pak and Cho [15] as well as Xuan and Roetzel [41] predict high specific heat capacities that are too high, resulting in relative deviations greater than 5%. With a decreasing nanoparticle size, the specific heat capacity of nanofluids decreases [55,59]. This is because the number of vibrational sources increases with decreasing particle size for the same volume concentration. The surface area per unit volume of small particles is greater than that of large particles. Therefore, Brownian motion and heat transfer are more active for small particles than for large particles, leading to an acceleration of heat transfer [55].
- The measured thermal diffusivity of W rises with increasing temperature by up to 8.6% at 318 K, while EG/W has a rise of 4.5%. Adding SiO_2 nanoparticles, the thermal diffusivity increases for 318 K and 20 wt.% SiO_2 to a maximum of 16.4% in W and 20.4% in EG/W, respectively.

- Equation (18) provides a maximum relative deviation of less than 1, 4, and 5% for the density, specific heat capacity, and thermal diffusivity, respectively.
- The calculated thermal conductivity shows a slight decrease of 3% in W and 1% in EG/W (25/75) at 5 wt.% SiO_2. With a higher concentration, it increases to a maximum at 20 wt.% SiO_2 with a rise of 9% for the base fluid W and 12% for the base fluid EG/W (25/75).
- The thermal conductivity is measured by various measuring devices. In this study, it is calculated by measuring the density, specific heat capacity, and thermal diffusivity. The decrease in the heat capacity in the low concentration range has a corresponding effect on the result for the thermal conductivity. With different geometries of the nanoparticles, the sphericity could also influence the thermal conductivity, which is shown in Equation (16). However, a more detailed analysis of sphericity with SEM images of different geometries would be necessary to examine this. In terms of the particle size, smaller particles lead to increased thermal conductivity due to increased Brownian motion.
- In comparison with other measuring devices, it has been found that the thermal conductivity values with the LFA are often lower than with the transient hot wire (THW) or hot disk method, for example [60–63]. Due to the low filling height of the sample of 0.5 mm (see Figure 6), the Brownian motion is inhibited, which is largely responsible for the increase in thermal conductivity in nanofluids [64,65]. As a result, the thermal conductivities differ depending on the application and are lower for heat transfer in a thin gap.

This study provides both the optical and thermophysical properties of both SiO_2 in W and SiO_2 in EG/W (25/75). In addition, a correlation is established for the measured variables as a function of the concentration and temperature, which works with only two adjustable parameters. This characterization of several thermophysical properties in combination with optical properties provides a simpler holistic analysis of the SiO_2 nanofluid compared to existing correlations in the literature. One limitation is that these measurements were made under static conditions. However, the temperature-dependent measurements provide important insights into how the nanofluid might behave under varying temperature conditions in a real system. In a dynamic state, such as in solar energy conversion systems, the continuous movement of the fluid can cause temperature fluctuations that can affect the efficiency of heat storage and transfer. Therefore, the temperature-dependent properties observed in the static experiments are an important step in assessing the suitability and performance of nanofluids in dynamic solar systems. A more detailed analysis depending on different flow patterns (laminar, transient, or turbulent) could only be carried out in further work.

In the future, further experimental data are also needed to close the gaps regarding the different material data properties and to gain a better understanding of the different nanofluid concentrations. In addition, the adjustable parameters of the presented correlations should be developed by physical relations to apply this approach to other nanofluids.

Author Contributions: Conceptualization, F.W. and Z.A.; methodology, F.W.; software, F.W.; validation, F.W., Z.A. and F.H.; formal analysis, F.W.; investigation, F.W.; data curation, F.W.; writing—original draft preparation, F.W.; writing—review and editing, Z.A, F.H. and D.B.; visualization, F.W.; supervision, D.B.; funding acquisition, F.H and D.B. All authors have read and agreed to the published version of the manuscript.

Funding: The authors of this work gratefully acknowledge the financial support provided by the Bavarian State Ministry of Education, Science, and Arts within the framework Graduiertenkolleg of the Technologie Allianz Oberfranken (TAO).

Data Availability Statement: The original data presented in the study are included in the article; further inquiries can be directed to the authors.

Acknowledgments: The authors would like to acknowledge Heider and the Bavarian Polymer Institute (BPI) for their support with the ZEISS LEA 1530 scanning electron microscope.

Conflicts of Interest: The authors declare no conflicts of interest. The funders had no role in the design of the study; in the collection, analyses, or interpretation of the data; in the writing of the manuscript; or in the decision to publish the results.

Abbreviations

Roman letters	
a	thermal diffusivity, (mm^2/s)
A, B	adjustable parameter in Equation (18)
A_V, B_V, C_V	adjustable parameter in Equation (14)
c_p	specific heat capacity (kJ/kgK)
I_0	initial radiation
I_T	radiation transmitted
k	thermal conductivity, (W/mK)
k′	wavenumber, (cm^{-1})
K_θ	calibration function
l_{ABS}	length of the absorption path, (cm)
m	mass, (kg)
n	number of data points
T	temperature, (K)
T_T	transmission, (-)
t_{50}	half-time of the temperature rise
u	uncertainties, (-)
V	volume, (m^3)
x_i	mass fraction liquid phase, (wt.%)
z	values, (-)
Greek letters	
α_{ext}	absorption coefficient, (cm^{-1})
β	shape factor, (-)
β_{hr}	heat rate
θ	heat flow rate, (W)
λ′	wavelength (nm)
ρ	density, (g/cm^3)
τ	oscillation period, (s)
φ	concentration
ψ	particle sphericity, (-)
Subscripts	
0	baseline
bf	base fluid
Calc	calculated
Exp	experimental
i	component index
nf	nanofluid
Np	nanoparticle
Ref	reference
S	sample
Abbreviations	
$Ag/CoSO_4$	silver nanoparticle in cobalt sulphate
Al_2O_3	aluminum oxide
Au	gold
Cu	copper
CuO	copper oxide
DMA	density meter
DSC	differential scanning calorimetry
EG	ethylene glycol
eq	equation

FT-IR	Fourier-transform infrared spectroscopy
LFA	laser flash analysis
PP	pressure pump
RD	relative deviation
RMSE	root mean square error
SiO_2	silicon dioxide
TiO_2	titanium dioxide
TPP	thermo-physical properties
VP	vacuum pump
W	water
ZnO	zinc oxide
ZrO_2	zirconium dioxide

References

1. Kabir, E.; Kumar, P.; Kumar, S.; Adelodun, A.; Kim, K.-H. Solar energy: Potential and future prospects. *Renew. Sustain. Energy Rev.* **2018**, *82*, 894–900. [CrossRef]
2. Gorji, T.B.; Ranjbar, A.A. A review on optical properties and application of nanofluids in direct absorption solar collectors (DASCs). *Renew. Sustain. Energy Rev.* **2017**, *72*, 10–32. [CrossRef]
3. Arthur, O.; Karim, M.A. An investigation into the thermophysical and rheological properties of nanofluids for solar thermal applications. *Renew. Sustain. Energy Rev.* **2016**, *55*, 739–755. [CrossRef]
4. Tembhare, S.P.; Barai, D.P.; Bhanvase, B.A. Performance evaluation of nanofluids in solar thermal and solar photovoltaic systems: A comprehensive review. *Renew. Sustain. Energy Rev.* **2022**, *153*, 111738. [CrossRef]
5. Okonkwo, E.C.; Wole-Osho, I.; Almanassra, I.W.; Abdullatif, Y.M.; Al-Ansari, T. An updated review of nanofluids in various heat transfer devices. *J. Therm. Anal. Calorim.* **2021**, *145*, 2817–2872. [CrossRef]
6. Choi, S.U.S. Enhancing thermal conductivity of fluids with nanoparticles. In *ASME International Mechanical Engineering Congress & Exposition*; Argonne National Lab: Argonne, IL, USA, 1995; Volume 29.
7. Mokhtarpour, M.; Homayoon-far, S.; Shekaari, H.; Zafarani-Moattar, M.T. Effect of Some Imidazolium-Based Ionic Liquids on the Stability, Volumetric, and Transport Properties of ZnO Nanofluids. *J. Chem. Eng. Data* **2020**, *65*, 5369–5383. [CrossRef]
8. Dey, D.; Kumar, P.; Samantaray, S. A review of nanofluid preparation, stability, and thermo-physical properties. *Heat Transf. Asian Res.* **2017**, *46*, 1413–1442. [CrossRef]
9. Zahmatkesh, I.; Sheremet, M.; Yang, L.; Heris, S.Z.; Sharifpur, M.; Meyer, J.P.; Ghalambaz, M.; Wongwises, S.; Jing, D.; Mahian, O. Effect of nanoparticle shape on the performance of thermal systems utilizing nanofluids: A critical review. *J. Mol. Liq.* **2021**, *321*, 114430. [CrossRef]
10. Zhong-Yong, Y.; Bao-Lian, S. Titanium oxide nanotubes, nanofibers and nanowires. *Colloids Surf. A Physicochem. Eng. Asp.* **2004**, *241*, 173–183. [CrossRef]
11. Vandrangi, S.K.; Hassan, S.; Sharma, K.V.; Akilu, S.; Emani, S.; Nabipour, N. Effect of base fluids on thermo-physical properties of SiO_2 nanofluids and development of new correlations. In *Mathematical Methods in the Applied Science*; Special Issue Paper; Wiley: Hoboken, NJ, USA, 2020; pp. 1–19. [CrossRef]
12. Wong, K.V.; De Leon, O. Applications of Nanofluids: Current and Future. *Adv. Mech. Eng.* **2010**, *2*, 519659. [CrossRef]
13. Talib, S.; Azmi, W.H.; Zakaria, I.; Mohamed, W.; Mamat, A.; Ismail, H.; Daud, W. Thermophysical Properties of Silicon Dioxide (SiO_2) in Ethylene Glycol/Water Mixture for Proton Exchange Membrane Fuel Cell Cooling Application. *Energy Procedia* **2015**, *79*, 366–371. [CrossRef]
14. Hashimoto, S.; Harada, M.; Higuchi, Y.; Matsunaga, T. Enhancement mechanism of convective heat transfer via nanofluid: An analysis by means of synchrotron radiation imaging. *Int. J. Heat Mass Transf.* **2020**, *159*, 120081. [CrossRef]
15. Pak, B.C.; Cho, Y.I. Hydrodynamic and Heat Transfer Study of Dispersed Fluids with Submicron Metallic Oxide Particle. *Exp. Heat Transf.* **1998**, *11*, 151–170. [CrossRef]
16. Ali, A.R.I.; Salam, B. A review on nanofluid: Preparation, stability, thermophysical properties, heat transfer characteristics and application. *SN Appl. Sci.* **2020**, *2*, 280. [CrossRef]
17. O'Hanley, H.; Buongiorno, J.; McKrell, T.; Hu, L. Measurement and Model Validation of Nanofluid Specific Heat Capacity with Differential Scanning Calorimetry. *Adv. Mech. Eng.* **2012**, *4*, 181079. [CrossRef]
18. Gupta, M.; Singh, V.; Kumar, R.; Said, Z. A review on thermophysical properties of nanofluids and heat transfer applications. *Renew. Sustain. Energy Rev.* **2017**, *74*, 638–670. [CrossRef]
19. Namburu, P.K.; Kulkarni, D.P.; Dandekar, A.; Das, D.K. Experimental investigation of viscosity and specific heat of silicon dioxide nanofluids. *Micro Nano Lett.* **2007**, *2*, 67–71. [CrossRef]
20. Vajjha, R.S.; Das, D.K. Specific heat measurement of three nanofluids and development of new correlation. *J. Heat Transf.* **2009**, *131*, 071601. [CrossRef]
21. Kwek, D.; Crivoi, A.; Duan, F. Effects of Temperature and Particle Size on the Thermal Property Measurements of Al_2O_3—Water Nanofluids. *J. Chem. Eng. Data* **2010**, *55*, 5690–5695. [CrossRef]

22. Tertsinidou, G.J.; Tsolakidou, C.M.; Pantzali, M.; Assael, M.J. New Measurements of the Apparent Thermal Conductivity of Nanofluids and Investigation of Their Heat Transfer Capabilities. *J. Chem. Eng. Data* **2016**, *62*, 491–507. [CrossRef]
23. Xie, H.; Chen, L. Review on the Preparation and Thermal Performances of Carbon Nanotube Contained Nanofluids. *J. Chem. Eng. Data* **2011**, *56*, 1030–1041. [CrossRef]
24. Bhandari, S.S.; Muralidhar, K.; Joshi, Y.M. Thermal Diffusivity and Viscosity of Suspensions of Disk-Shaped Nanoparticles. *Ind. Eng. Chem. Res.* **2013**, *52*, 15114–15123. [CrossRef]
25. Sahoo, B.C.; Das, D.K.; Vajjha, R.S.; Satti, J.R. Measurement of the Thermal Conductivity of Silicon Dioxide Nanofluid and Development of Correlations. *J. Nanotechnol. Eng. Med.* **2012**, *3*, 041006. [CrossRef]
26. Ferrouillat, S.; Bontemps, A.; Ribeiro, J.-P.; Gruss, J.-A.; Soriano, O. Hydraulic and heat transfer study of SiO_2/water nanofluids in horizontal tubes with imposed wall temperature boundary conditions. *Int. J. Heat Fluid Flow* **2011**, *32*, 424–439. [CrossRef]
27. Dong, J.; Zheng, Q.; Xiong, C.; Sun, E.; Chen, J. Experimental investigation and application of stability and thermal characteristics of SiO_2-ethylene-glycol/water nanofluids. *Int. J. Therm. Sci.* **2022**, *176*, 107533. [CrossRef]
28. Rejvani, M.; Alipour, A.; Vahedi, S.M.; Chamkha, A.J.; Wongwises, S. Optimal characteristics and heat transfer efficiency of SiO_2/water nanofluid for application of energy devices: A comprehensive study. *Int. J. Energy Res.* **2019**, *43*, 8548–8571. [CrossRef]
29. Mukherjee, S.; Panda, S.R.; Mishra, P.C.; Sen, S.; Chaudhuri, P. Thermophysical and transient heat transfer characteristics of aqueous SiO_2 nanofluid in energy management applications. *J. Process Mech. Eng.* **2022**, *237*, 1100–1111. [CrossRef]
30. Guo, Y.; Zhang, T.; Zhang, D.; Wang, Q. Experimental investigation of thermal and electrical conductivity of silicon oxide nanofluids in ethylene glycol/water mixture. *Int. J. Heat Mass Transf.* **2018**, *117*, 280–286. [CrossRef]
31. Otanicar, P.T.; Phelan, P.E.; Golden, J.S. Optical properties of liquids for direct absorption solar thermal energy systems. *Sol. Energy* **2009**, *83*, 969–977. [CrossRef]
32. Taylor, R.A.; Otanicar, P.T.; Rosengarten, G. Nanofluid-based optical filter optimization for PV/T systems. *Light Sci. Appl.* **2012**, *1*, e34. [CrossRef]
33. Han, X.; Chen, X.; Wang, Q.; Alelyani, S.M.; Qu, J. Investigation of $CoSO_4$-based Ag nanofluids as spectral beam splitters for hybrid PV/T applications. *Sol. Energy* **2019**, *177*, 387–394. [CrossRef]
34. Khullar, V.; Bhalla, V.; Tyagi, H. Potential Heat Transfer Fluids (Nanofluids) for Direct Volumetric Absorption-Based Solar Thermal Systems. *J. Therm. Sci. Eng. Appl.* **2018**, *10*, 011009. [CrossRef]
35. Huber, M.; Harvey, A.; Lemmon, E.; Hardin, G.; Bell, I.; McLinden, M. Reference Fluid Thermodynamic and Transport Properties Database (REFPROP) Version 10-SRD 23. NIST2018. Available online: https://data.nist.gov/od/id/725039AC054648F9E0532457068156CB1948 (accessed on 8 October 2024).
36. Bohren, C.F.; Huffman, D.R. *Absorption and Scattering of Light by Small Particles*; John Wiley & Sons: Hoboken, NJ, USA, 1998.
37. Anton Paar GmbH. *Operating Instructions Density Meter 4200 M*; Anton Paar GmbH: Tokyo, Japan, 2017.
38. Netzsch Gerätebau GmbH. *Operating Instructions DSC Apparatus DSC 200 F3 Maia*; Netzsch Gerätebau GmbH: Selb, Germany, 2012.
39. Höhne, G.W.H.; Hemminger, W.F.; Flammersheim, H.-J. *Differential Scanning Calorimetry*, 2nd ed.; Springer: Berlin/Heidelberg, Germany, 2003.
40. Netzsch Gerätebau GmbH. *Operating Instructions Nano-Flash-Apparatus LFA 447*; Netzsch Gerätebau GmbH: Selb, Germany, 2012.
41. Xuan, Y.; Roetzel, W. Conceptions for heat transfer correlation of nanofluid. *Int. J. Heat Mass Transf.* **2000**, *43*, 3701–3707. [CrossRef]
42. Esfe, M.H.; Afrand, M. An updated review on the nanofluids characteristics. *J. Therm. Anal. Calorim.* **2019**, *138*, 4091–4101. [CrossRef]
43. Pietrak, K.; Wisniewski, T.S. A review of models for effective thermal conductivity of composite material. *J. Power Technol.* **2015**, *95*, 14–24.
44. Maxwell, J.C. *A Treatise on Electricity and Magnetism*; Macmillan & Co. Ltd.: New York, NY, USA, 1881.
45. Hamilton, R.L.; Crosser, O.K. Thermal Conductivity of Heterogeneous Two-Component Systems. *Div. Ind. Eng. Chem.* **1962**, *1*, 3. [CrossRef]
46. Karami, M.; Raisee, M.; Delfani, S.; Akhavan Bahabadi, M.A.; Rashidi, A.M. Sunlight Absorbing Potential of Carbon Nanoball Water and Ethylene Glycol-Based Nanofluids. *Opt. Spectrosc.* **2013**, *3*, 400–405. [CrossRef]
47. Sharma, T.; Rani, R.; Kumar, A.; Bamezai, R.K. Solution properties of an antidiabetic drug metformin hydrochloride in aqueous urea and thiourea solutions: A physicochemical study. *J. Mol. Liq.* **2020**, *300*, 111985. [CrossRef]
48. Shi, Y.; Zhu, C.; Fu, T.; Gao, X.; Ma, Y. Volumetric and Viscometric Properties of Maltitol in Glycylglycine Aqueous Solutions at T = 293.15–333.15 K. *J. Chem. Eng. Data* **2021**, *66*, 360–367. [CrossRef]
49. Moosavi, M.; Rostami, A.A. Densities, Viscosities, Refractive Indices, and Excess Properties of Aqueous 1,2-Etanediol, 1,3-Propanediol, 1,4-Butanediol, and 1,5-Pentanediol Binary Mixtures. *J. Chem. Eng. Data* **2017**, *62*, 156–168. [CrossRef]
50. Arnautovic, Z.; Kutzner, S.; Weith, T.; Heberle, F.; Brüggemann, D. Density and Viscosity of Linear Siloxanes and Their Mixtures. *J. Chem. Eng. Data* **2023**, *68*, 314–329. [CrossRef]
51. Nan, Z.; Liu, B.; Tan, Z. Calorimetric investigation of excess molar heat capacities for water + ethylene glycol from T = 273.15 to T = 373.15 K. *J. Chem. Thermodyn.* **2002**, *34*, 915–926. [CrossRef]
52. Zhang, X.; Gu, H.; Fujii, M. Experimental study on the effective thermal conductivity and thermal diffusivity of nanofluids. *Int. J. Thermophys.* **2006**, *27*, 569–580. [CrossRef]

53. Balderas-Lopez, J.A.; Mandelis, A.; Garcia, J.A. Measurements of the Thermal Diffusivity of Liquids with a Thermal-Wave Resonator Cavity. *Anal. Sci./Suppl.* **2001**, *17*, s519–s522. [CrossRef]
54. Eckert, E.R.; Drake, R.M.J.R. Analysis of Heat and Mass Transfer. 1987. Available online: https://www.osti.gov/biblio/7142648 (accessed on 8 October 2024).
55. Zhang, L.; Zhang, A.; Jing, Y.; Qu, P.; Wu, Z. Effect of Particle Size on the Heat Transfer Performance of SiO_2—Water Nanofluids. *J. Phys. Chem. C* **2021**, *125*, 13590–13600. [CrossRef]
56. Pantzali, M.M.; Kanaris, A.G.; Antoniadis, K.D.; Mouza, A.A.; Paras, S.V. Effect of nanofluids on the performance of a miniature plate heat exchanger with modulated surface. *Int. J. Heat Fluid Flow* **2009**, *30*, 691–699. [CrossRef]
57. Kotia, A.; Borkakoti, S.; Deval, P.; Ghosh, S.K. Review of interfacial layer's effect on thermal conductivity in nanofluid. *Heat Mass Transf.* **2017**, *53*, 2199–2209. [CrossRef]
58. Bird, R.B.; Stewart, W.E.; Lightfoot, E.N. *Transport Phenomena*; John Wiley & Sons: New York, NY, USA, 2011.
59. Shahrul, I.M.; Mahbubul, I.M.; Khaleduzzaman, S.S.; Saidur, R.; Sabri, M. A comparative review on the specific heat of nanofluids for energy perspective. *Renew. Sustain. Energy Rev.* **2014**, *38*, 88–98. [CrossRef]
60. Buonomo, B.; Colla, L.; Fedele, L. A comparison of nanofluid thermal conductivity measurements by flash and hot disk techniques. In Proceedings of the 32nd UIT Heat Transfer Conference, Pisa, Italy, 23–25 June 2014; Volume 547, p. 012046. [CrossRef]
61. Zagabathuni, A.; Ghosh, S.; Pabi, S.K. The difference in the thermal conductivity of nanofluids measured by different methods and its rationalization. *Beilstein J. Nanotechnol.* **2016**, *7*, 2037–2044. [CrossRef]
62. Aparna, Z.; Michael, M.M.; Pabi, S.K.; Ghosh, S. Diversity in thermal conductivity of aqueous Al_2O_3- and Ag-nanofluids measured by transient hot-wire and laser flash methods. *Exp. Therm. Fluid Sci.* **2018**, *94*, 231–245. [CrossRef]
63. Palacios, A.; Cong, L.; Navarro, M.E.; Ding, Y.; Barreneche, C. Thermal conductivity measurement techniques for characterizing thermal energy storage materials—A review. *Renew. Sustain. Energy Rev.* **2019**, *108*, 32–52. [CrossRef]
64. Krishnamurthy, S.; Bhattacharya, P.; Phelan, P.E.; Prasher, R.S. Enhanced Mass Transport in Nanofluids. *Nano Lett.* **2006**, *6*, 419–423. [CrossRef] [PubMed]
65. Jang, S.P.; Choi, S.U.S. Role of Brownian motion in the enhanced thermal conductivity of nanofluids. *Appl. Phys. Lett.* **2004**, *84*, 4316–4318. [CrossRef]